Journal of Applied Fluid Mechanics, Vol. 12, No. 1, pp. 195-205, 2019.
Available online at www.jafmonline.net, ISSN 1735-3572, EISSN 1735-3645.
DOI: 10.29252/jafm.75.253.29090

Experimental Investigation and ANN Prediction on the Underbody Drag Minimization in Truck Model using DC Pulsed DBD Plasma Actuator as an Active Flow Control Device

A. Sangeet Sahaya Jeyangel[1†] and J. Jancirani[2]

[1] *Department of Automobile Engineering, Madras Institute of Technology Campus, Anna University, Chromepet, Chennai, Tamilnadu, India*
[2] *Department of Production Technology, Madras Institute of Technology Campus, Anna University, Chromepet, Chennai, Tamilnadu, India*

†*Corresponding Author Email: sangeet@mitindia.edu*

(Received April 10, 2018; accepted July 24, 2018)

ABSTRACT

Copious researches have been accomplished in the realm of automotive aerodynamics leading to the reduction of drag in cars, trucks and buses. The overwhelming results have further spearheaded the present work in emphasizing the underbody drag minimization of distribution trucks using plasma actuator as an active flow control technique. Four different types of plasma actuators also called Active Side Skirt were experimentally evaluated on the scale down model of truck in a subsonic wind tunnel along with five different voltages ranging from 12 kV to 28 kV. The plasma actuator was positioned on the sides of the truck vertically as four individual units covering the front tyres and rear tyres. The results exhibit that the plasma actuator with a larger insulated electrode and with an electrode overlap distance had a good drag reduction rate of 8% at higher velocity (28 kV).The plasma generated by the Active Side Skirt induces an ionic wind along the stream wise direction keeping the flow attached throughout thereby helping in a reduced drag. An artificial neural network was developed using the data from the experimental analysis with Voltage, Velocity, Top width, Bottom width and Overlap distance as input parameter for training the network, further coefficient of drag taken as output parameter. A total of two hidden layers and seven neurons was used for the prediction. The test data that was not used for training, correlated with the ANN predicted value furthermore with the experimental values.

Keywords: Underbody drag; Truck; Artificial neural network; Plasma Actuator; Active flow control; Active Side skirt; Drag reduction.

NOMENCLATURE

AFC	Active flow control technique	L_t	length of top electrode
ANN	Artificial Neural Network	PA_1, PA_2, PA_3, PA_4	active side skirt 1,2,3,4
ASS	Active Side Skirt	R_e	Reynold's number
C_{DF}	coefficient of drag	*RSS*	Rear Side Skirt
C_{LF}	coefficient of lift	*S*	thickness of dielectric medium
d_o	electrode overlap distance		
FSS	Front Side Skirt	*t*	electrode thickness
H	height of active side skirt	V_w	flow velocity
HVPG	High Voltage Plasma Generator	W_b	width of Insulated Electrode
L_b	length of insulated electrode	W_t	width of Top Electrode
L_p	plasma length		

1. INTRODUCTION

The aerodynamic drag has been on focus as a domain for researchers and industrial experts with aim of diminution in fuel consumption and emission for a decade. There is still room for improvement with the world moving towards cleaner and greener environment. The heavy vehicles, trucks being the

major consumers of diesel can still be made more fuel efficient with the improvements in aerodynamic design, reducing the overall weight and by downsizing the engine. The improvements in aerodynamic design, being a concrete idea can be executed by flow control devices without going for the latter ideas. Sovran (1983) investigated and found that the reduction of 10% of aerodynamic drag resulted in 3% increase in fuel savings, thus establishing the influence of drag on fuel saving. The first phase of the paper investigates the effect of drag on a truck model and the influence of an active flow control retrofitting device in reducing the underbody drag. The four principal areas concentrated to reduce drag-the front region, the gap region, the underbody and rear region of the trucks are the main source of drag for fore body drag, gap drag, underbody drag and base drag Wood (2006).In agreement with Wood (2006) the underbody drag constituting about 30% of the total drag in trucks had garnered more prominence, as it is the contributing factor for base drag i.e. the negative pressure created on the rear end of a vehicle. Gopal *et al.* (2013) also investigated the effect of reducing the flow separation downstream in a car model to reduce drag. Lo *et al.* (2017) studied the effect of flow separation at the end of a tractor trailer and found out the counter clockwise rotating wake vortex at the rear end of the trailers influences the flow separation of the trailer. When the flow of air interacts on the lacuna below the truck it induces vortical activities which make up the major source of drag which cannot be neglected Choi *et al.* (2014). Hwang *et al.* (2016) had experimentally investigated that when flap type of side skirt, bent inwards were utilized in 15-ton scale modelled truck, the pressure difference near the rear wheels had been reduced with decrease in turbulent kinetic energy leading to a 5% reduction in coefficient of drag. Kim *et al.* (2017) also investigated the effect of flap type side skirt for underbody flow using PIV technique and achieved 6% drag reduction in trucks.

The active flow control devices had also gained importance in reducing drag as it regulates stability of air flow using small input energy Jahanmiri (2010).Furthermore active flow control devices control complex flow structure. De Giorgi *et al.* (2016) achieved a reduction of 14% diminution in pressure loss coefficient using micro Plasma Actuator and also reported that increase in voltage juxtaposed a reduction in the pressure loss. Moreau (2007) had reported that the electric winds created by the plasma formation on the DBD plasma actuator directed span wise manipulated the surrounding air with less input power and suggested that plasma should act at the right time and location. Roy *et al.* (2016) demonstrated the, use of plasma actuator for reducing the base drag and achieved 10 % reduction in aerodynamic drag at speed of 31.21 m/s for a scaled tractor-trailer model, but the power needed to actuate the plasma actuator was 4.5 times more than power saved, so there arises a need to design an efficient plasma actuator which is on par with the passive flow control devices with the aim of reducing drag. The dielectric barrier discharges based plasma actuators that had been created are with AC HV supply and had been presented by (Yokoyama *et al.* 1990 and Fridman *et al.* 2005).

The investigation extends to the second phase with first being the experimental analysis of the underbody drag, the latter involves using Artificial Neural Network (ANN) to predict and validate the experimental results. The ANN is propitious in establishing a correlation between the input and output data to establish a predictive output ANN model Bhowmik *et al.* (2017). Syed *et al.* (2017) had investigated various transfer function combination (tansig-tansig, logsig-tansig, tansig-logsig, logsig-logsig logsig-purelin tansig-purelin purelin-logsig purelin-tansig) and found, tansig-tansig transfer function combination had good performance when compared to other transfer function .Rezaei *et al.*(2015) reported that Levenberg–Marquardt algorithm has an extremely good convergence and is quicker than the other algorithm. The feed-forward back propagation methodology of neural network was used to predict up to five output parameters by Roy *et al.* (2014) with precise results. The contemporary literatures that are divulged above substantiate the possibility of exercising ANN as propitious tool for mapping intricate input, and output parameters with the aid of tansig-tansig transfer function and Levenberg–Marquardt algorithm.

The present investigation embarks on a possible way to exploit the methods of actuating DBD Plasma actuator with pulsed – Dc supply as an active flow control technique to reduce the aerodynamic underbody drag on a truck model and further engages in developing an ANN model with a scanty data evaluated experimentally on a wind tunnel, which can effectively predict the coefficient of drag.

2. MODELS AND MEASUREMENT

2.1 Vehicle Model and Drag Measurement

The present investigation revolves around underbody drag reduction mainly in distribution trucks. The truck model , scaled down to 1/16 scale with a dimension of 0.52 m, 0.17 m, 0.265 m length, width, height respectively as shown in Fig. 2.a has been used to study the influence of active flow control devices. The blockage ratio was found to be 6% which according to West *et al.* (1982) does not influence the measured drag coefficient and pressure distribution. The pressure distribution for the model was measured using a 64 channel digital pressure scanner, on the pressure tapping points drilled on the surface. The pressure probes were installed throughout the symmetry plane of the model and taken out via the floor of the model so that there is minimal flow disturbance. The pressure tapping points were equally spaced with more numbers evenly spread on the underside of the truck model to capture the under flow.

The wind tunnel used for testing the model was an open type subsonic wind tunnel with a test section of 2.0 m in length 1.2 m in width and 1.0 m in height. The maximum air speed was limited to 50 m/s. The free stream velocity was measured using a hot wire

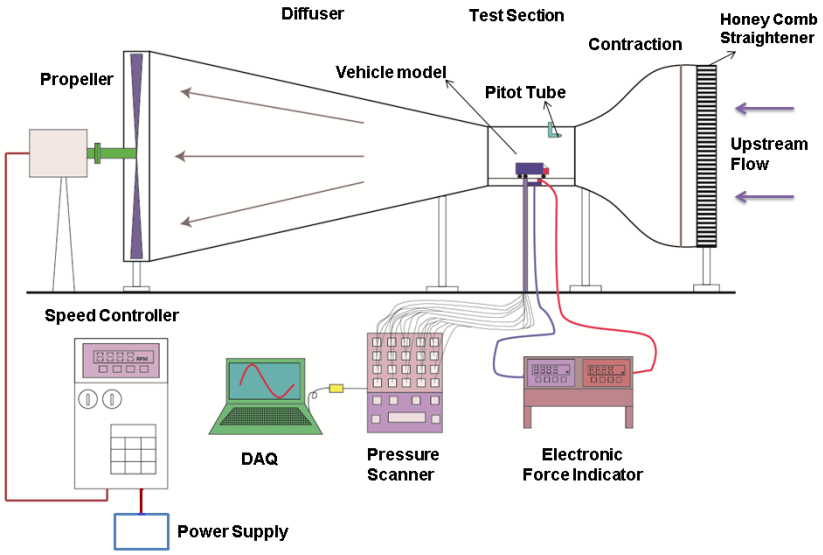

Fig. 1. Schematic Representation of experimental setup.

anemometer which was located at a distance 0.25 m from the top floor of the test section and 0.25 m from the front of the model. The contraction ratio of the wind tunnel was 9:1. The floor of the test section was fixed which was satisfactory for investigating the flow effects on ground vehicle Hucho *et al.* (1975). The temperature was retained at 27^0 -31^0C inside the test section of the wind tunnel. The freestream turbulent intensity of the wind tunnel was 0.4%.

Fig. 2.a. Photograph of the truck model.

The aerodynamic force created on the model with respect to the air velocity was measured using a cantilever type double load cell setup with individual indicators for measuring Drag Force which acted on the direction of travel of the air and Lift Force which acted perpendicular to the model along Y axis, digitally. The load cell setup was affixed below the bottom plate of the test section, with the model coupled to the load cell using a U Clamp on the bottom plate of the test section. The schematic representation illustrating the model along with the wind tunnel is manifested in Fig. 1. The cross wind flow effect was not taken into account and drag coefficient was evaluated with 0^0 yaw angle using the equations (1) and (2)

$$C_{DF} = F_{DF}/(0.5 \times \rho \times A \times V_w^2) \quad (1)$$

$$C_{LF} = F_{LF}/(0.5 \times \rho \times A \times V_w^2) \quad (2)$$

Where F_{DF} and F_{LF} is the drag and lift force measured along the direction of air flow, A is the model frontal cross section area, ρ and V_w are the density and velocity of air, C_{DF} and C_{LF} are the coefficient of drag and lift force measured using the above equation.

2.2 Estimation of Uncertainty

The instruments used in experimental analysis to measure drag parameters are prone to few errors while measuring or due to its calibration which is unavoidable but has to be taken care. To check the repeatability of the measured value, uncertainty analysis is calculated using root mean square methodology on the basis of each individual instrument analysis. The total uncertainty analysis U was calculated using equation (3) Paul, A, *et al.* (2013).

Uncertainty of Experiment conducted

$$= \sqrt{\left(\frac{\partial U}{dx_1} \mathrm{x}\ \Delta \mathrm{X}_1\right)^2 + \left(\frac{\partial U}{dx_2} \mathrm{x}\ \Delta \mathrm{X}_2\right)^2 + \cdots \ldots + \left(\frac{\partial U}{dx_n} \mathrm{x}\ \Delta \mathrm{X}_\mathrm{n}\right)^2} \quad (3)$$

Where x_1, x_2 ,..... x_n indicates the independent variables such as drag force and pressure and ΔX_1, ΔX_2,.... ΔX_n represents the errors of the variables . The calculated percentage of uncertainty for coefficient of drag is ±1.45% and for coefficient of pressure is ± 0.86% and is tabulated as shown in Table 1

2.3 Design of Active Side Skirt

The truck model was attached to an active flow control device to modify the flow of air in the regions covering the front and rear wheels and the underbody of truck. The Active Flow Control device employed for investigation was a Single Dielectric Barrier Discharge Plasma Actuator (SDBD) Roy, *et al.* (2016) implanted on the side of the truck which runs vertically as two individual units on both the sides, intended to perform the function of side skirt. The

Table 1 Total % of uncertainty for the parameters

Parameter	Variable	Measuring Instruments	% of uncertainty of Measuring Instruments	Calculation	Total % of uncertainty
Coefficient of Drag	Drag Force	a) Load cell	0.6	$\sqrt{[(a^2)+(b^2)+(c^2)+(d^2)]}$	1.45
		b) Load cell indicator	0.5		
		c) Anemometer	0.7		
		d) Frontal area calculation	1		
Coefficient of Pressure	Pressure	e) Pressure Scanner	0.5	$\sqrt{[(e^2)+(f^2)]}$	0.86
		f) Anemometer	0.7		

front and rear Plasma Actuator are located after the front and rear tyres arrangement respectively. The Plasma Actuator is provided with a pulsed Direct current with a high voltage in the order of 10-28 kV. The main benefits of using a SDBD Plasma Actuator are faster response time, negligible mass and no moving elements.

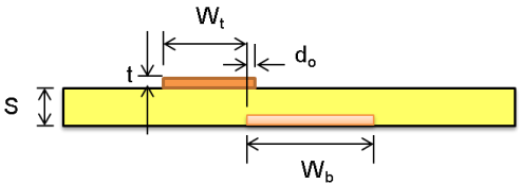

Fig. 2.b. Side view of Active Side Skirt.

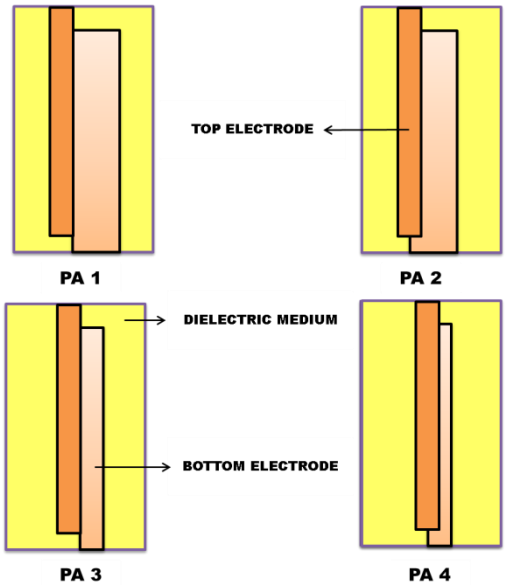

Fig. 2.c. Top view of the four configuration of Active Side Skirt.

The SDBD is embodied of a dielectric medium with two electrodes etched on the top and bottom layer of the dielectric of which the bottom electrode should be an encapsulated with a kapton tape and the top one as an exposed electrode. The two electrodes are provided with a pulsed DC power supply

Four configurations of Plasma Actuator hereby called Active Side Skirt (ASS) were used for the investigation namely PA_1, PA_2, PA_3, PA_4 which have been illustrated in Fig. 2.c. The height of Active Side Skirt (H) was set as 81 mm, taking into consideration the minimum ground clearance as 20 cm with (H) kept constant throughout for all the four types of ASS. The electrode was made of copper tape with thickness for both top and insulated electrode (t) as 60 µm. Acrylic was used as the dielectric medium with a thickness (S) of 1 mm. The top and insulated electrode is covered using a 50 µm kapton tape for preventing reverse discharge and to act as resistance to high voltages. The entire four configurations have a top electrode width (W_t) of 6 mm. The first and the second configuration PA_1 and PA_2 have an insulated electrode width (W_b) of 12 mm respectively along with the third and the fourth configuration PA_3 and PA_4 having a width (W_b) of 6 mm. According to Post *et al.* (2004), for getting more uniform plasma along the actuator the electrode overlap distance (d_o) was set to 0.5 mm for PA_2 and PA_4 , however for PA_1 and PA_4 there was no overlap. Figure 2.b. represents the side view of the Active Side Skirt.

2.4 Plasma Generating Device and Test Setup

The ASS was actuated using pulsed DC supply with the help of dedicated High Voltage Plasma Generator (HVPG) and PWM controller as a prime source of electric power. The HVPG is capable of generating higher electrical potential of range 10 to 30 kV being supplied with conventional AC power source as input. In most of the previous studies, the plasma actuators were electrified with high potential AC source and its plasma generation efficiency was studied and reported. In the present work the active side skirt actuators are designed based on the (Vernet, J.A. *et al.* 2015 and Cattafesta III, L.N *et al.* 2011) design recommendation being formulated earlier and it is supplied with DC pulsed source taking into account of essential engineering and cost reduction factors such as accessibility and production of higher voltage DC being quite easier and cheaper when compared to AC source. Furthermore the efficiency of the plasma generation using DC supply is slightly higher when compared to the actuators which were supplied with AC as a power source. The outline of plasma generating device used in this study is portrayed in Fig. 2.d. and the principle behind the generation of pulsed DC supply is shown in Fig. 2.e.

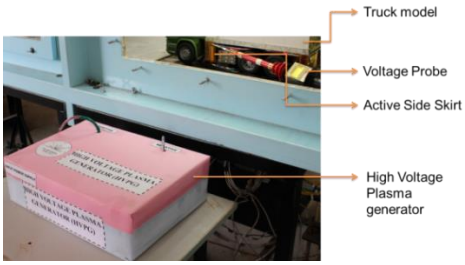

Fig. 2.d. HVPG with the truck model.

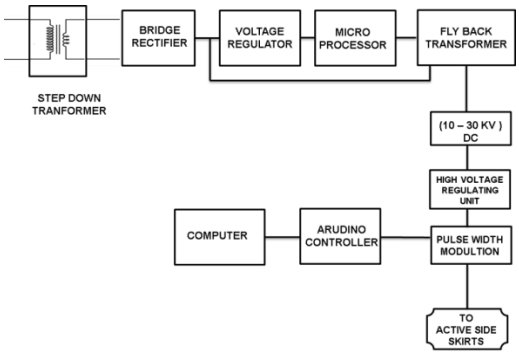

Fig. 2.e. Layout involving the working of HVPG.

3. RESULTS

3.1. Experimental Investigation Results

3.1.1 Coefficient of Drag

The truck model was evaluated without any retrofitting devices for a wind speed of 10 m/s to 50 m/s and the drag coefficient of the model was found to be indistinguishable throughout the velocity range. The drag coefficient of the reference model at wind speed v_w = 30 m/s was 0.791 as indicated in the Fig. 3.a. The Reynolds number (R_e) for the truck model at wind speed v_w = 30 m/s was calculated based on the equation Shankar *et al.* 2018 shown below and the value was 1.246×10^6 which is similar to the standard critical Reynolds number.

$$R_e = \frac{\rho_a \times l \times V_w}{\mu} \quad (4)$$

Where $\boldsymbol{l}$ represents length of the truck model, $\boldsymbol{V_w}$ wind speed, $\boldsymbol{\rho_a}$ density of air, and finally $\boldsymbol{\mu}$ kinematic viscosity of air.

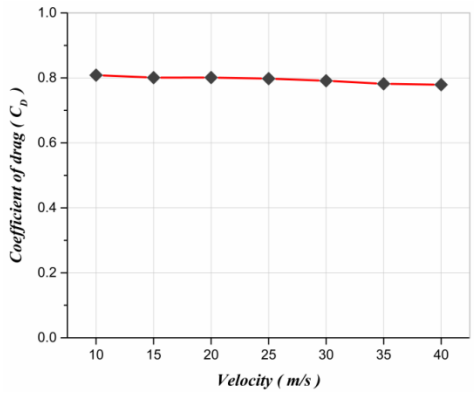

Fig. 3.a.Variation of coefficient of drag for reference model.

3.1.2 Variation of Drag Force

The readings from the electronic force indicator noted as drag force F_D for the reference model, clearly pointed out the proportionality of the drag force and velocity. In particular the drag force increasing with the square of velocity, illustrated in the Fig. 3.b can be easily visualized. The scale downed reference model tested in the wind tunnel thus proves to be a precise one as that of a full scale testing.

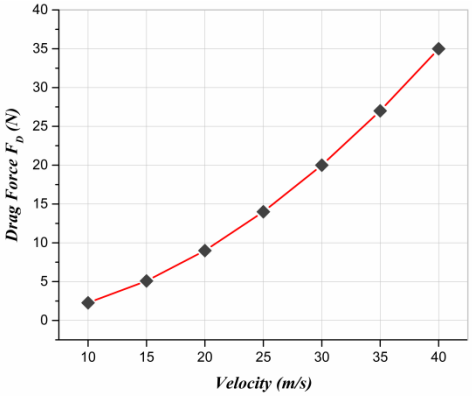

Fig. 3.b. Drag force variation for reference model.

3.1.3 Drag Reduction Rates

Four different types of Active Side Skirt PA $_1$, PA $_2$, PA $_3$, PA $_4$ were tested on the reference model to discover the best promising Active Side Skirt, contributing to maximum underbody drag reduction. The four combination of Active side skirt were also tested for distinct voltage supplies from the High Voltage Plasma generator. The combination of distinct voltage with distinct ASS design was performed on discrete velocity ranging from 10 m/s to 50 m/s. The coefficient of drag reduction rate for voltage range 12 kV to 28 kV with an increment of 4 has been studied and is illustrated in the Fig. 3.c – 3.g. It was found that the voltage had direct impact on the drag coefficient reduction rate with both being directly proportional. The maximum drag reduction percentage was achieved using PA_2 Active Side Skirt which has a d_o of 0.5mm and a greater W_b for all the voltage range when stacked up against the other ASS design. Around 8% coefficient of drag reduction rate was achieved using the PA_2 ASS at a voltage of 28 kV that substantiated the assertion, higher the voltage, higher the reduction in % drag reduction rate. However voltage greater than 28 kV could not be achieved due to physical constraints in developing and maintaining voltage from High Voltage Plasma Generator and thus ASS was tested up to set voltage (28 kV).

The results are prodigious on comparing with the other active flow control device like fluidic oscillator where 6.8 % drag reduction was achieved El-Alti, M *et al.* (2012).

The pressure drag being the main source of drag in heavy vehicle, instigates flow separation caused mainly by the pressure difference and formulates the

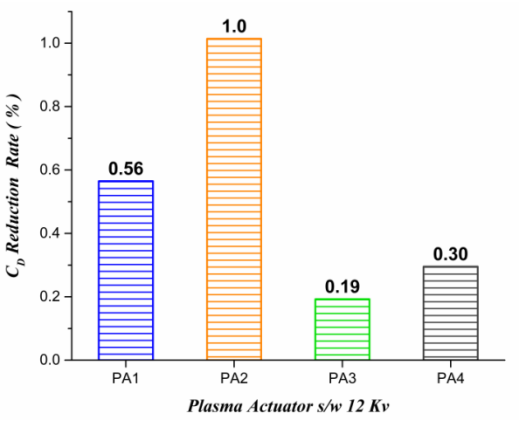

(3.c)

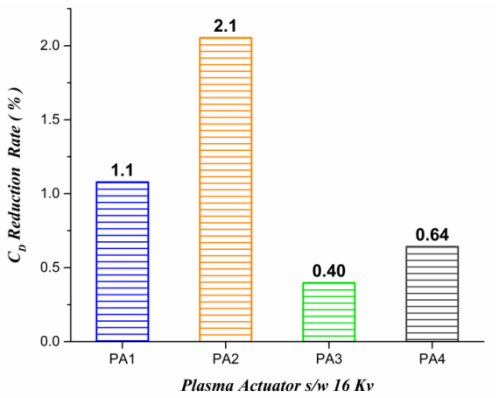

(3.d)

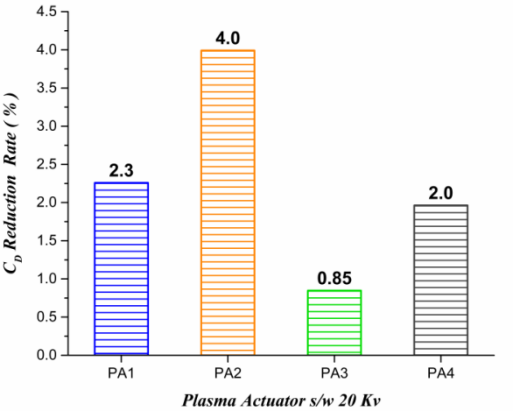

(3.e)

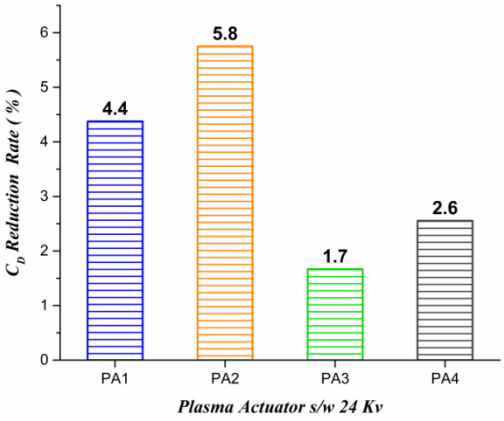

(3.f)

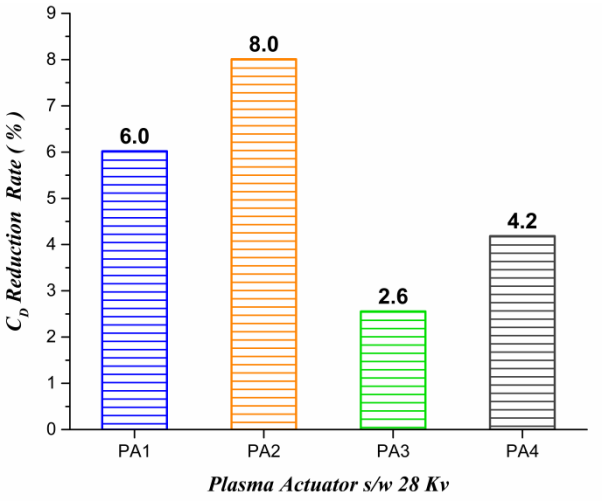

(3.g)

Fig. 3.c – 3.g Comparison of Drag coefficient reduction rate w.r.t to reference model for different types of ASS in relation to discrete voltages.

flow to decelerate and forms low velocity wake region leading to under body drag formation that was subjugated by fitting the truck model with ASS. The air flow induced by the electrostatic forces termed as coronal wind was produced between the top and the insulated electrode of the ASS by the application of high voltage along the span wise direction of the ASS ionizes the air, thereby generating a purple coloured plasma jet which can be noticed in the Fig. 3.i. when the plasma in ON condition. The plasma keeps the flow attached to the areas of front tyre and near the rear tyres where the ASS has been placed span wise. The vortex formation is reduced by streamlining the air flow in these areas and the flow which gets separated near the wheels when passed along the top electrode gets reattached leading to an increase in pressure juxtaposing the wake region. This reduction in pressure difference ultimately reduces the drag on the vehicle. This phenomenon also causes adverse effect on the rear of vehicle leading to diminution in

base drag to some extent. The Active Side Skirt (ASS) constitutes two units, the front part called Front Side Skirt (FSS) and rear part called Rear Side Skirt (RSS).The FSS and RSS secured to the truck model collectively contributed to the total drag reduction. The individual contribution of the both ASS was investigated on the PA_2 which had the maximum coefficient of drag reduction rate. Furthermore to investigate the effect regarding the position of FSS and RSS, the truck model was tested experimentally for three cases. Power supply from the HVPG to the FSS was switched on and the supply to the RSS was switched off deliberately and the truck model was tested considering it to be the case I. It was found that a meagre 2% drag reduction was achieved during the testing. The case II was tested with the RSS in ON mode and FSS in OFF mode conversely to case I, and 6.7% drag reduction was achieved as illustrated in the Fig. 3.h. Case III which is the combination of both the FSS and RSS had been tested previously. Comparative results provide easy insight that the maximum drag reduction of 8% was achieved combining the FSS and RSS, subsequently both FSS and RSS reduce drag in a similar way.

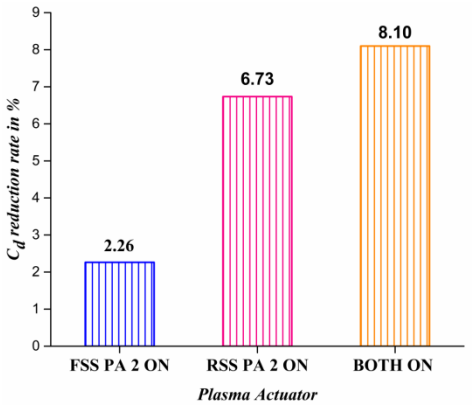

Fig. 3.h. Position of ASS influencing the coefficient of drag reduction rate.

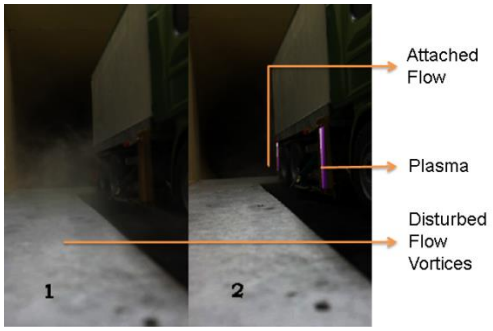

Fig. 3.i. Flow visualization (a) ASS OFF (b) ASS ON.

Small drag reduction of 2% achieved using FSS exhibits that the flow entering the areas near the front tyres is off high pressure making a reduced pressure gradient leading to a reduced drag reduction rate consequently the air builds a recirculation region near the rear wheels increasing the pressure and leads to an increase in drag overcoming the effect of using the FSS as there is no RSS to control the air flow at the rear section.

In the case II, air flow entering the areas of rear tyres when passing through the RSS gets altered by the plasma jet making a narrow downed recirculation region near the rear tyres. The recirculation region generated due to the flow separation and formation of turbulent eddies near the rear tyres for the model without any retrofitting device is reduced due to the presence of ASS. This reduced recirculation region increases the pressure surrounding leading to a reduced pressure gradient which ultimately leads to reduced drag of about 6.73%.

3.2 Smoke Visualization

The air flow patterns near the areas of Active Side Skirts were visualized using smoke generator which is a commonly practised flow visualization technique. The stream of invisible air containing the clue to the promising active flow control device is injected with smoke by blowing it near the separated flow.

The figure illustrates the visualization results at (25 m/s). The smoke was introduced into the areas near the front and rear tyres where the flow separates and forms vortices. The vortical activities near the rear wheels, increase the pressure difference and ultimately lead to wake region formation and build the underbody drag. The 1 part of the Fig. 3.i represents Active Side Skirt fixed to the side walls of the truck in OFF condition and 2 part of the Fig. 3.i represents Active Side Skirt in ON condition. The wake structure difference between the ASS in ON and OFF conditions provides simple and more perspicuous explanation in the reduction of vortices formation owing to the pressure difference by the Active Side Skirt when activated , clearly influencing the reduction of underbody drag . PIV measurement could show more insight to study the other influencing factors.

3.3. ANN Prediction

3.3.1. Instigation of ANN Model

The Artificial Neural Network, a computational model, based on neural network Ghobadian *et al.* (2009) was stimulated using MATLAB for predicting the coefficient of under body drag. The general working of Artificial Neural Network is illustrated as flowchart in the Fig. 3.k. The input parameters fed to input layer of ANN model yields an input signal to the hidden layer which supplies the corresponding signal to the output layer through which the output of the model is projected. In the present investigation an ANN model was instigated with feed-forward back propagation with Levenberge Marquardt learning algorithm (trainlm) to predict the output parameter as it has minimal error when compared to other neural networks and utilized by the researchers to predict results with accuracy.

The pictorial representation of the network architecture is shown in Fig. 3.j. A single model was developed based on the experimental data, with an amalgamation of five voltages, four velocities, and four Plasma actuator design configurations

Table 2 Parameters for ANN model

Topology	(5-7-1)
	5 Inputs
	1 Output
	1 Hidden layer
	7 Neuron
Training Algorithm	TRAINLM (Levenberge Marquardt)
Activation function	Log – sigmoid
Training Data	70 % of the sample (56 patterns)
Testing Data	15% of the sample (12 patterns)
Validation Data	15% of the sample (12 patterns)

amounting to a total of 80 samples of which 70 % of the sample (56 patterns) were alloted for training the neural network and the remaining 30% of the sample (24 patterns) were set aside for validation and predictions. Before feeding the samples to the network, the data are normalized from 0.1 to 0.9 using the equation (5) shown below and then randomized.

Normalized value =

$$\left\{(U_L - L_L) X \left(\frac{\text{Experimental}_{Actual} - \text{Experimental}_{Min}}{\text{Experimental}_{Max} - \text{Experimental}_{Min}}\right) + L_L\right\} \quad (5)$$

$$MSE = \frac{1}{s} X \{\sum_1^s (x_i - z_i)^2\} \quad (6)$$

$$R = \sqrt{\left[1 - \left\{\frac{\sum_1^s (x_i - z_i)^2}{\sum_1^s z_i^2}\right\}\right]} \quad (7)$$

Where U_L, L_L represents the upper and lower limit of the value, s represents the number of output data, similarly x_i and z_i indicates the experimental and ANN predicted output data

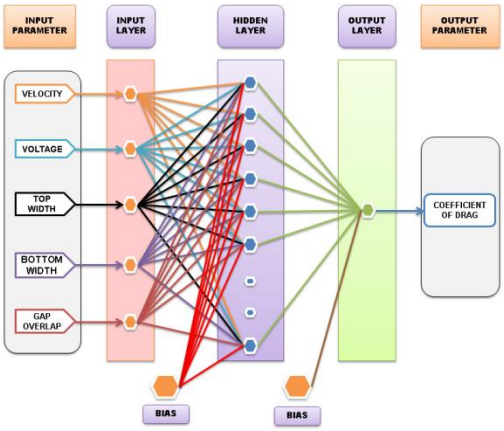

Fig. 3.j. Schematic diagram of network architecture.

The table 2 represents the network model with one input, hidden and output layers each, with 5 inputs and 1 output parameter. The five input parameters taken into account were Velocity, Voltage, Top width, Bottom width and Gap overlap.

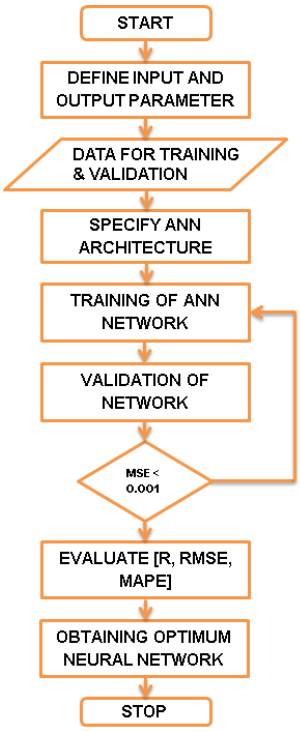

Fig. 3.k. Flowchart of Artifical Neural Network.

The mentioned input parameters are embodied into the ANN model since it is capable of covering the domain. Similarly coefficient of drag was considered as an output parameter for a perfect architecture.

The ANN model was first trained with a hidden layer and number of neurons ranging from two to twenty-five neurons according to the previous investigations by Roy *et al.* (2014) and Bhowmik *et al.* (2017). The numbers of neurons were increased and the output of the network was compared with the set output and checked for minimum value of MSE. The variation

in number of neuron with MSE was plotted as indicated in Fig. 3.l. The minimum MSE value of 0.0001 was obtained with 7 neurons

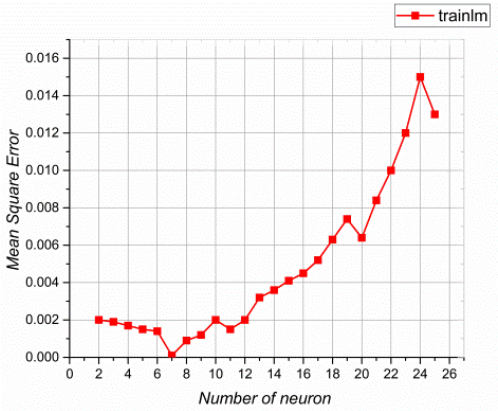

Fig. 3.l. Variation of number of neuron with MSE.

3.3.2. Modelling Result

The optimal ANN model was devised in concurrent with the other pertinent research studies with the upper limits for Mean Absolute percentage error (MSE) as 5%, Regression coefficient (R) greater than 0.98 and Mean Square Error (MSE) less than 0.001. The neural network was trained till the optimal model was reached and finally validated with the experimental data.

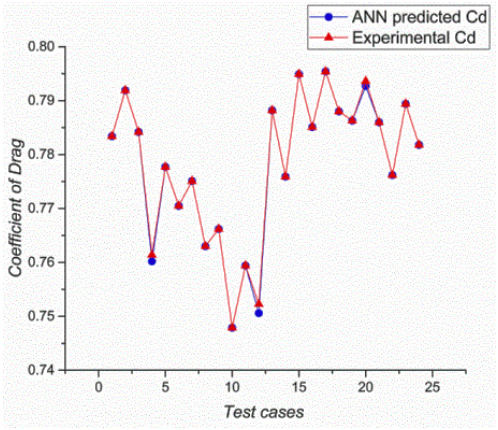

Fig. 3.m. Comparision of ANN predicted C_d with Experimental C_d.

The predicted ANN output data yielded impressive correlation with the experimental values which are indicated in the Fig. 3.m. and could be easily visualized. The proficiency of the ANN model is attributed to the ability of the neural network to relearn, for improved performance. The comparison of the experimentally measured coefficient of drag with the ANN predicted Coefficient of drag yielded MSE, MAPE and regression coefficient value of the order 0.0037, 1.76% and 0.99649 with trainlm algorithm, and 7 neurons.

The regression plot after de-normalization illustrated in the Fig. 3.n. shows the strong association between the actual experimental values and the ANN predicted values. Furthermore the regression coefficient of the ANN model is 0.99893 for training 0.99533 for testing 0.99348 for validation and overall coefficient of 0.99649. It is evident that artificial neural network is fast, simple, accurate and reliable in predicting the values without failures.

The higher regression coefficient directly induces the accuracy of the predicting ANN model. The computational ANN model has been developed to predict the experimental data with minimum Mean Square Error (MSE) and maximum Regression coefficient which exhibits that ANN can be used to predict drag coefficient with ease and less time without performing experiments for all the cases in further studies.

4. Discussion And Concluding Remarks

The underbody drag in distribution truck caused by the flow around the front, rear section of tyres and the underbody was experimentally analysed using Active Side Skirts as an active flow control device and furthermore predicted using ANN for different voltage, velocity and varied Plasma Actuator side skirt design and the concluding remarks are summarized below.

1) The maximum recorded drag coefficient reduction rate among the four Active Side Skirts was PA_2 with a reduction rate of 8% as compared to the model without retrofitting device.

2) The flow structure propounds that Active Side Skirts reduced drag by modifying the flow near the wheel region and reduced the pressure difference, momentum loss and vortices formations.

3) The voltage and the dimensions of the Active Side Skirts were the most prominent factors influencing the drag coefficient.

4) The active flow control technique was on a par with the passive technique in terms of drag reduction.

5) Both FSS and RSS of the Active Side Skirts contributed to the total drag reduction rate with RSS being the superior one.

6) The results clearly demonstrated that the training algorithm of feed forward back-propagation was sufficient in predicting the coefficients of drag.

7) The gross Regression coefficient and Mean squared error for the ANN model were 0.99649 and 0.0037, respectively.

8) The predicted values of ANN were in line with experimental values which demonstrated that ANN could be used to simulate and validate the coefficient of drag for underbody drag reduction.

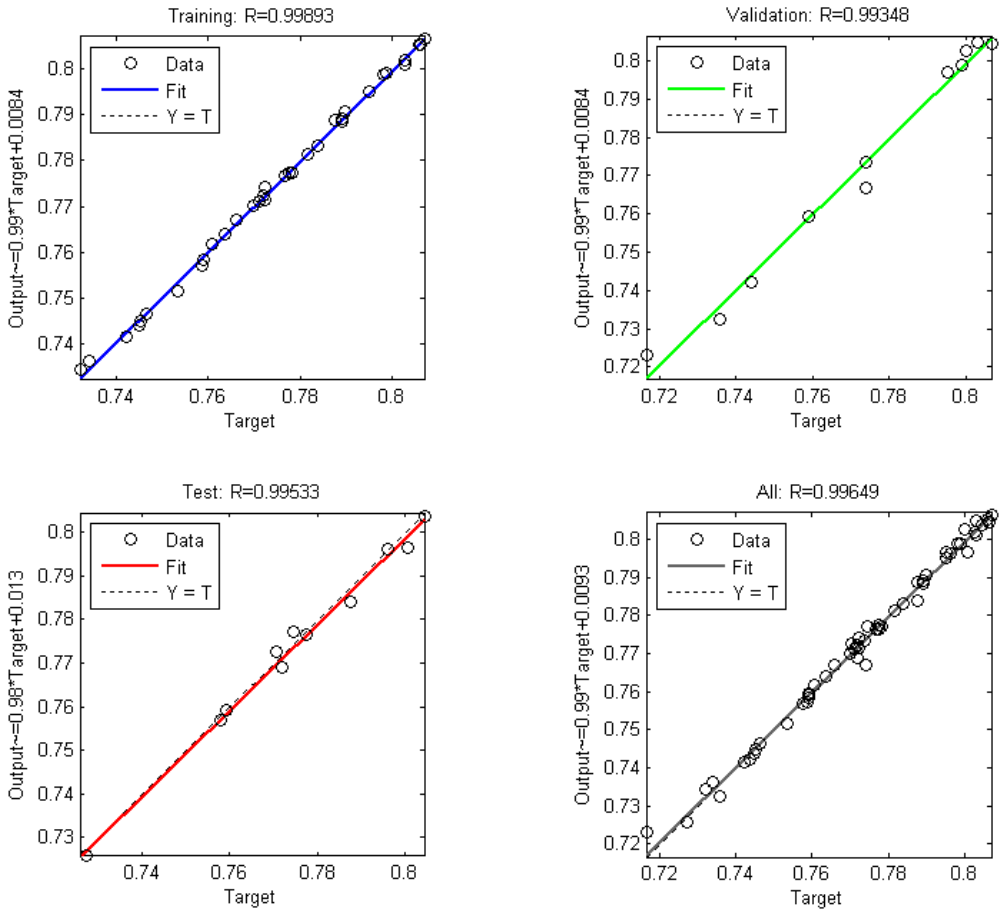

Fig. 3.n. Overall Correlation coefficient of developed neural network.

The contemporary investigation evinces that, DC pulsed actuated Plasma Actuator (Active Side Skirt) with larger insulated electrode compared to the top electrode and with an overlap distance of 0.5mm (PA2) can be used as a retrofitting device for underbody drag reduction in trucks.

ACKNOWLEDGEMENTS

The author wishes to express his gratitude to the Centre for Research, Anna University, Chennai, Tamil Nadu, India for their support.

REFERENCES

Bhowmik, S., R. Panua, D. Debroy and A. Paul (2017). Artificial Neural Network Prediction of Diesel Engine Performance and Emission Fueled With Diesel–Kerosene–Ethanol Blends: A Fuzzy-Based Optimization. *Journal of Energy Resources Technology*. 139(4), 042201.

Cattafesta III, L. N. and M. Sheplak (2011). Actuators for active flow control. *Annual Review of Fluid Mechanics*. 43, 247-272.

Choi, H., J. Lee and H. Park (2014). Aerodynamics of heavy vehicles. Annual Review of Fluid Mechanics. 46, 441-468.

De Giorgi, M. G., E. Pescini, F. Marra and A. Ficarella, (2016). Plasma actuator scaling down to improve its energy conversion efficiency for active flow control in modern turbojet engines compressors. *Applied Thermal Engineering*. 106, 334-350.

El-Alti, M., V. Chernoray, M. Jahanmiri and L. Davidson (2012). Experimental and computational studies of active flow control on a model truck-trailer. *EPJ Web of Conferences.* EDP Sciences. 25, 01012.

Fridman, A., A. Chirokov and A. Gutsol (2005). Non-thermal atmospheric pressure discharges. *Journal of Physics D: Applied Physics*. 38(2), R1.

Ghobadian, B., H. Rahimi, A. M. Nikbakht, G. Najafi and T. F. Yusaf (2009). Diesel engine performance and exhaust emission analysis using waste cooking biodiesel fuel with an artificial neural network. *Renewable Energy*. 34(4), 976-982.

Gopal, P. and T. Senthilkumar (2013). Influence of Wake Characteristics of a Representative Car Model by Delaying Boundary Layer Separation. *Journal of Applied Science and Engineering*. 16(4), 363-374.

Hucho, W.H., L.J. Janssen and G. Schwarz (1975). The wind tunnel's ground floor boundary layer—its interference with the flow underneath cars. *SAE Paper*.750066.

Hwang, B. G., S. Lee, E. J. Lee, J. J. Kim, M. Kim, D. You and S. J. Lee (2016). Reduction of drag in heavy vehicles with two different types of advanced side skirts. *Journal of Wind Engineering and Industrial Aerodynamics.* 155, 36-46.

Jahanmiri, M. (2010). *Active flow control: a review*.

Kim, J. J. and S. J. Lee (2017). Drag-reducing underbody flow of a heavy vehicle with side skirts. *Journal of Visualization*. 20(2), 369-378.

Lo, K. H. and K. Kontis (2017). Flow around an articulated lorry model. *Experimental Thermal and Fluid Science*. 82, 58-74.

Moreau, E. (2007). Airflow control by non-thermal plasma actuators. *Journal of physics D: applied physics*. 40(3), 605.

Paul, A., P. K. Bose, R. S. Panua and R. Banerjee (2013). An experimental investigation of performance-emission trade off of a CI engine fueled by diesel–compressed natural gas (CNG) combination and diesel–ethanol blends with CNG enrichment. *Energy*. 55, 787-802.

Post, M. L. and T. C. Corke (2004). Separation control on high angle of attack airfoil using plasma actuators. *AIAA journal*. 42(11), 2177-2184.

Rezaei, J., M. Shahbakhti, B. Bahri and A. A. Aziz (2015). Performance prediction of HCCI engines with oxygenated fuels using artificial neural networks. *Applied Energy*. 138, 460-473.

Roy, S., P. Zhao, A. DasGupta and J. Soni (2016). Dielectric barrier discharge actuator for vehicle drag reduction at highway speeds. *AIP Advances*. 6(2), 025322.

Roy, S., R. Banerjee and P. K. Bose (2014). Performance and exhaust emissions prediction of a CRDI assisted single cylinder diesel engine coupled with EGR using artificial neural network. *Applied Energy*. 119, 330-340.

Shankar, G. and G. Devaradjane (2018). Experimental and Computational Analysis on Aerodynamic Behavior of a Car Model with Vortex Generators at Different Yaw Angles. *Journal of Applied Fluid Mechanics*. *11*(1).

Sighard F. Hoerner. (1950). Base drag and thick trailing edges. *Journal of the Aeronautical Sciences, 17*(10),622-628.

Sovran, G. (1983). Tractive-energy-based formulae for the impact of aerodynamics on fuel economy over the EPA driving schedules. *SAE Technical Paper*. 830304.

Syed, J., R. U. Baig, S. Algarni, Y. S. Murthy, M. Masood and M. Inamurrahman (2017). Artificial Neural Network modeling of a hydrogen dual fueled diesel engine characteristics: An experiment approach. *International journal of hydrogen energy*. 42(21), 14750-14774.

Vernet, J. A., R. Örlü and P. H. Alfredsson (2015). Separation control by means of plasma actuation on a half cylinder approached by a turbulent boundary layer. *Journal of Wind Engineering and Industrial Aerodynamics*. 145, 318-326.

West, G. S. and C. J. Apelt (1982). The effects of tunnel blockage and aspect ratio on the mean flow past a circular cylinder with Reynolds numbers. *Journal of Fluid mechanics*. 114, 361–377.

Wood, R.M. (2006).A discussion of a heavy truck advanced aerodynamic trailer system. In: *9th international symposium on heavy vehicle weights dimensions*, University Park, PA, USA

Yokoyama, T., M. Kogoma, T. Moriwaki and S. Okazaki (1990). The mechanism of the stabilisation of glow plasma at atmospheric pressure. *Journal of Physics D: Applied Physics*. 23(8), 1125.